Integrative Biology

Cite this: *Integr. Biol.*, 2012, **4**, 422–430

www.rsc.org/ibiology

PAPER

Hyaluronic acid matrices show matrix stiffness in 2D and 3D dictates cytoskeletal order and myosin-II phosphorylation within stem cells†‡

Florian Rehfeldt,*[ab] André E. X. Brown,[a] Matthew Raab,[a] Shenshen Cai,[a] Allison L. Zajac,[a] Assaf Zemel[c] and Dennis E. Discher*[a]

Received 31st October 2011, Accepted 12th January 2012
DOI: 10.1039/c2ib00150k

Physical features of microenvironments such as matrix elasticity E can clearly influence cell morphology and cell phenotype, but many differences between model matrices raise questions as to whether a standard biological scale for E exists, especially in 3D as well as in 2D. An E-series of two distinct types of hydrogels are ligand-functionalized here with non-fibrous collagen and used to elucidate wide-ranging cell and cytoskeletal responses to E in both 2D and 3D matrix geometries. Cross-linked hyaluronic acid (HA) based matrices as well as standard polyacrylamide (PA) hydrogels show that, within hours of initial plating, the adhesion, asymmetric shape, and cytoskeletal order within mesenchymal stem cells generally depend on E nonmonotonically over a broad range of physiologically relevant E. In particular, with overlays of a second matrix the stiffer of the upper or lower matrix dominates key cell responses to 3D: the cell invariably takes an elongated shape that couples to E in driving cytoplasmic stress fiber assembly. In contrast, embedding cells in homogeneous HA matrices constrains cells to spherically symmetric shapes in which E drives the assembly of a predominantly cortical cytoskeleton. Non-muscle myosin II generates the forces required for key cell responses and is a target of a phospho-Tyrosine signaling pathway that likely regulates contractile assemblies and also depends nonmonotonically on E. The results can be understood in part from a theory for stress fiber polarization that couples to matrix elasticity as well as cell shape and accurately predicts cytoskeletal order in 2D and 3D, regardless of polymer system.

[a] *Biophysical Eng'g. Lab, University of Pennsylvania, Philadelphia 19104, PA, USA. E-mail: discher@seas.upenn.edu; Tel: +1 215 898 4809*
[b] *3rd Institute of Physics—Biophysics, Georg-August-University, Friedrich-Hund-Platz 1, 37077 Göttingen, Germany. E-mail: rehfeldt@physik3.gwdg.de; Fax: +49 551 397720; Tel: +49 551 3913831*
[c] *Institute of Dental Sciences, Faculty of Dental Medicine, and the Fritz Haber Center for Molecular Dynamics, the Hebrew University-Hadassah Medical Center, Jerusalem 91120, Israel*

† Published as part of an iBiology themed issue entitled "From Single Cells to Biology" Editors: Dr Mina Bissell, Distinguished Scientist, and Prof. Luke Lee.

‡ Electronic supplementary information (ESI) available: Standard cell biology methods and suppl. figures. See DOI: 10.1039/c2ib00150k

Introduction

Matrix elasticity influences many aspects of cell behavior including morphology,[1–4] motility,[5] and even processes as complex as differentiation.[4,6] Understanding the mechano-sensitivity to micro-environments seems key to deeper insight into clinically relevant processes[7] ranging from tumor growth [8] and wound healing[9] to cell therapies.[10,11] Such studies have thus far suggested the potency of matrix relative to soluble factors[6,9,12] and have demonstrated a key role for the force-generating acto-myosin cytoskeleton—at least for human mesenchymal stem cells (hMSCs) being widely applied in cell therapy.[13] Past studies have also converged on the physiological range of soft tissue elasticity

Insight, innovation, integration

A naturally derived, polyanionic hydrogel and a second, fully synthetic, neutral hydrogel are functionalized with collagen, crosslinked to give the same elasticity E, and shown to cause the same morphological and cytoskeletal responses of adult stem cells over a two order magnitude, in the physiological range of E. Cytoskeletal polarization modeled by a force dipole embedded in or on elastic matrices fits the nonmonotonic trends in both 2D and 3D cultures, thus demonstrating that E is a key biophysical parameter independent of matrix composition.

E = 0.1 kPa to 100 kPa, which is much softer than glass or plastic dishes but still broad in range. Moreover, cells in tissues are often surrounded by a matrix in 3D—as opposed to conventional 2D cultures, all of which motivate the integrative studies here of cell morphology and myosin in various 2D and 3D matrix systems.

The most commonly used hydrogel to study matrix elasticity effects is polyacrylamide (PA) as introduced by Pelham and Wang,[2] who demonstrated significant differences in cell behavior and phospho-Tyrosine signaling on 'stiff' *versus* 'soft' substrates. PA hydrogels as well as polydimethylsiloxane (PDMS) films[13–15] generally impact the cytoskeleton,[6,15] but these matrix systems are not sufficiently biocompatible for control over elasticity and ligand density in full 3D cultures. More traditional 3D matrix systems already in use for years such as collagen matrices[16] or matrigel[17] do not permit the tunability needed to understand the separate effects on the cytoskeleton of matrix elasticity *versus* ligand density *versus* fibrillar topography. Overlays of matrix (*e.g.* collagen I) on 2D cultures are nonetheless useful since stratified 3D microenvironments are evident in tissues such as the muscle stem cell niche, where satellite cells reside between the muscle fiber and the basal lamina in experiencing distinct matrix compositions on their basal and apical surfaces.[18] To generate space-filling matrices of well-defined elasticity and with ligand control, one could choose from many biocompatible polymerizations. Modified versions of naturally derived hyaluronic acid (HA) have become a popular choice (*e.g.* ref. 19), but HA matrices need to be carefully engineered and analyzed at the micro-level for well-controlled experiments on the adhesive and cytoskeletal responses in 3D culture.

The thiol-modified hyaluronic acid here (HA-S in Fig. 1A), which we introduced several years ago,[19] enables accurate control of hydrogel elasticity E and ligand density. It also enables 3D cell culture either with matrix overlays or by embedding cells during HA polymerization (Fig. 1B). Prior chemistries of a similar type did not encompass the physiological range of E,[20] nor did they exhibit fine tunability in E,[21] although very recent efforts with HA appear equally promising (*e.g.* ref. 22). By adapting previous protocols[23–26] for thiol modification of HA employing a mono-functional addition group instead of the disulfide-containing dihydrazides and by using a higher molecular weight HA (M_w = 413 kDa) as well as a higher crosslinker density, we achieve a finely tunable E from 0.1 to 100 kPa, thus covering a broad physiological range.[6,7,19] Cultures of hMSCs on or in these gels ultimately demonstrate that broken symmetry states and acto-myosin organization are dictated by matrix elasticity in 2D as well as 3D.

Results and discussion

Adhesive integration of cytoskeleton with matrix in 2D, 3D

AFM topography and immunofluorescence imaging of the same hMSC on a stiff collagen-coated PA gel (Fig. 1C) shows no visible collagen fibrils on the gel. Immunofluorescence of collagen-I also shows intercalation in the gel (to ~1 μm) but no obvious fibrillar structure (Fig. 1D). In contrast, immunostaining of nonmuscle myosin-IIA confirms within the cell an abundance of stress fibers, locally aligned. The rightmost images highlight the adhesive integration of such stress fibers into the matrix, consistent with traction force propagation from the cell to the substrate.[6]

When cells are allowed to attach and spread on a collagen-coated PA gel and then HA-gelatin is poured on top of the cells all on the same day, the cells are seen in confocal imaging (Fig. 1D images) to be conformally embedded within the sandwich gel system, engaging the matrix that surrounds the cell. Both HA and PA hydrogels are predominantly water and do not adversely impact optical resolution. Indeed, the rightmost confocal image sections clearly show both apical and basal stress fibers of actin–myosin and also the actin-binding, focal adhesion protein vinculin. In 2D, the apical surface shows very few vinculin adhesions within the same cell that exhibits prototypical adhesions at the basal surface (Fig. 1D, plot). However, within the 3D overlays, apical adhesions of vinculin are more than twice as abundant and similar to adhesion densities on the basal surface of cells in 2D and 3D. This is the first of multiple measures below that show cells do not distinguish up from down in these 3D systems.

Fine tuning matrix elasticity E

Our focus is on the cell, but matrix details need to be explained because a cell—especially a highly programmable stem cell—can be remarkably sensitive to the microenvironment. Thiol modified HA (HA-S) was prepared by a method extended from Shu *et al.*,[23] with the degree of substitution (d.s.) of added thiol groups determined by ^{1}H NMR to be d.s. = 0.76 (Fig. S1, ESI‡). Mixing HA-S with polyethyleneglycol-diacrylate (PEG-DA) as a crosslinker yields an elastic hydrogel within one hour. E of these gels was determined (see Methods) by force-indentation measurements in phosphate buffered saline (PBS) with an atomic force microscope (AFM),[27] and the resulting curves (*e.g.* Fig. S2A, ESI‡) were fitted with a modified Hertz model.[28] Increasing the ratio of cross-linkers to thiol at constant HA-S concentration produces an increase in E up to an optimal ratio above which E decreases with further cross-linker (Fig. 2A, left plot). The first regime is linear ($R^2 > 0.99$) as expected from rubber elasticity theory,[29] and the subsequent decrease in elasticity is readily explained by the bifunctional nature of PEG-DA. An effective crosslink forms only if both acrylate groups bind to a thiol group (–SH); at PEG-DA/SH ratios approaching $\frac{1}{2}$, there are fewer and fewer thiol groups left to react. This leads to dangling PEG chains that not only limit effective cross-links but soon compete against productive crosslinks and thereby decrease matrix stiffness.

The second parameter that can be used to tune the elasticity is the concentration of HA-S. The rightmost plot in Fig. 2A shows the elasticity of hydrogels made at varying concentrations of HA-S while maintaining a constant PEG-DA/HA-S ratio. An increase in weight percent of HA-S leads to a higher value of E that fits to strong scaling:

$$E \approx (c - c_0)^{\alpha}$$

with α = 2.6 and a critical concentration for gelation of c_0 = 0.4 w/v%. The parameters are well within the range of reported exponents for other crosslinked polymer networks.[30] Additional bulk rheology measurements show excellent agreement with the microscopic AFM data and also show that the elastic

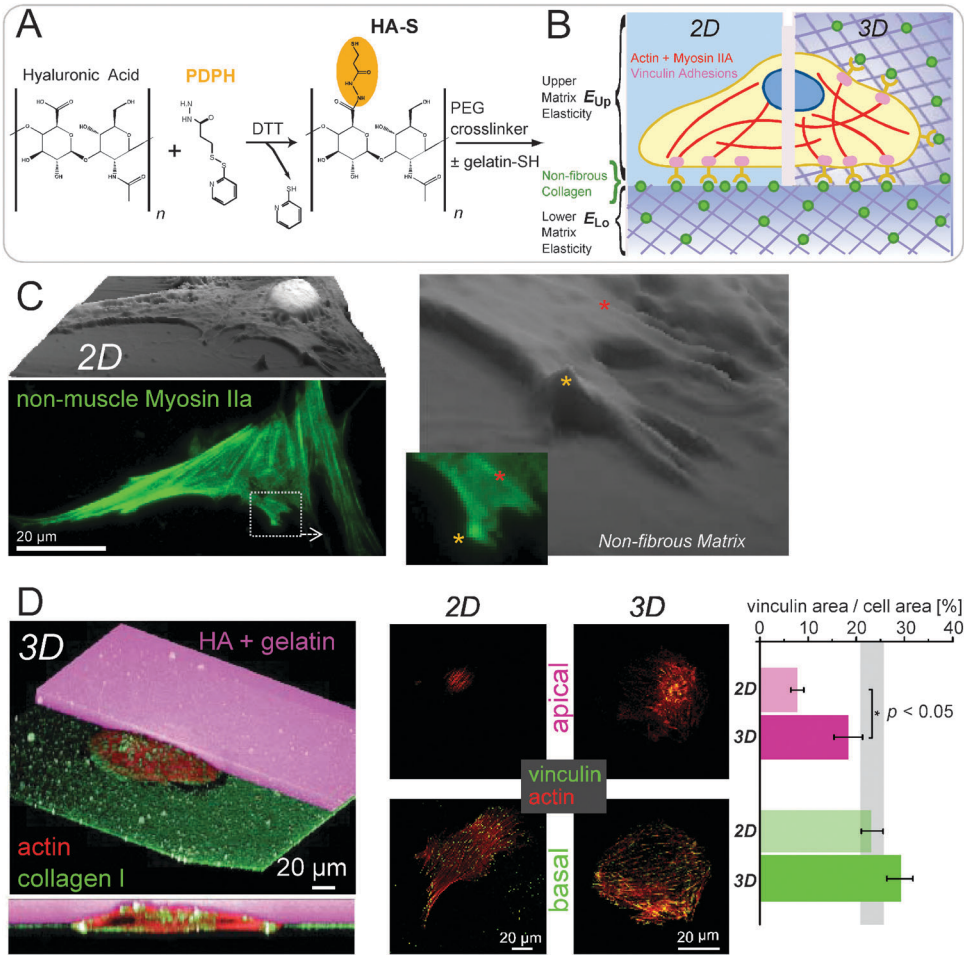

Fig. 1 Elastic HA matrices permit probing of the cytoskeletal order and adhesive integration in 2D and 3D. (A) Reaction scheme for thiol modification of hyaluronic acid (HA). PDPH is coupled to the carboxyl group of HA using carbodiimide chemistry at pH 4.75. Subsequent reduction of the disulfide bond of PDPH using dithiothreitol (DTT) at pH 8.5 yields HA with functional thiol groups shaded in orange (HA-S) that is crosslinked with PEG-DA with and without thiol-modified gelatin (gelatin-SH). (B) The left side of the sketch depicts a cell on a conventional 2D substrate (PA/HA hydrogel) of elasticity E_{Lo} (lower matrix elasticity). To enable cell adhesion, the matrix is coated with adhesion ligands (green circles: non-fibrous collagen I or gelatin-SH). The right side shows a 3D environment created by a conformal overlay with a hydrogel of elasticity E_{Up} (upper matrix elasticity). (C) AFM contact mode image of a human mesenchymal stem cell (hMSC) on a collagen I coated 2D gel substrate (E = 34 kPa) showing the smooth, homogeneous, non-fibrillar surface of the hydrogel and the fibrous structure of the cytoskeleton spanning the cell and nucleus. The lower image shows the corresponding immuno-fluorescence image of the same cell's cytoskeleton. Scale bar is 20 µm. Zooming further in shows anchorage of the stress fibers onto a relatively homogenous, flat substrate. (D) (Left) 3D image of a cell (stained for actin in red, collagen I in green, and the HA–gelatin hydrogel overlay in purple) in a 3D sandwich gel imaged with a laser scanning confocal microscope exhibiting a conformal overlay of the top gel and the localization of collagen to the surface of the lower gel. A thiol-reactive probe only stained the upper gel not the cell or the bottom gel as illustrated in the cross-section below the main image. (Middle) confocal slices of the cell's apex and base showing the actin cytoskeleton (red) and vinculin (green) to visualize focal adhesions. (Right) quantification of the ratio of the vinculin area to the cell area yields a significant difference between the apex in 2D and 3D, demonstrating that focal adhesions on the cell apex are only present in the 3D environment. Scale bars are 20 µm.

response dominates the viscous response. For 3D culture systems it is essential to mix matrix ligands into the hydrogel as they cannot be coated afterwards. Incorporation of 1% gelatin-SH stiffens the HA gels (as an evident crosslinker) but produces the same scaling exponent with lower c_0.

Several days after preparation, a significant increase of stiffness is measurable (Fig. S2B, ESI‡), and reflects disulfide crossbridging (S–S) as also reported by other groups.[20,23] The characteristic time constant τ for this hardening process is on the order of 1 day, and is reversible by disulfide reduction with DTT. To prevent this continuous stiffening and to achieve a stable gel we capped the thiol groups in the gels (in two hour reactions) either with a 1.5% solution of iodoacetamide in PBS or, if living cells were present as in 3D gels, with 2% cysteine in PBS. After inactivation, the mechanical properties remained stable (closed circles in Fig. S2B, ESI‡), even after culturing cells for 24 to 48 hours (as below) and even when probed by AFM near the cells. Moreover, since the initially attached collagen has no detectable effect on E,[3] any secreted or adsorbed matrix is also unlikely to impact E. Three parameters thus tune the elasticity E of HA-S hydrogels: the ratio of cross-linkers to thiol groups, the concentration of HA-S, and the time at which the remaining free thiol groups are inactivated.

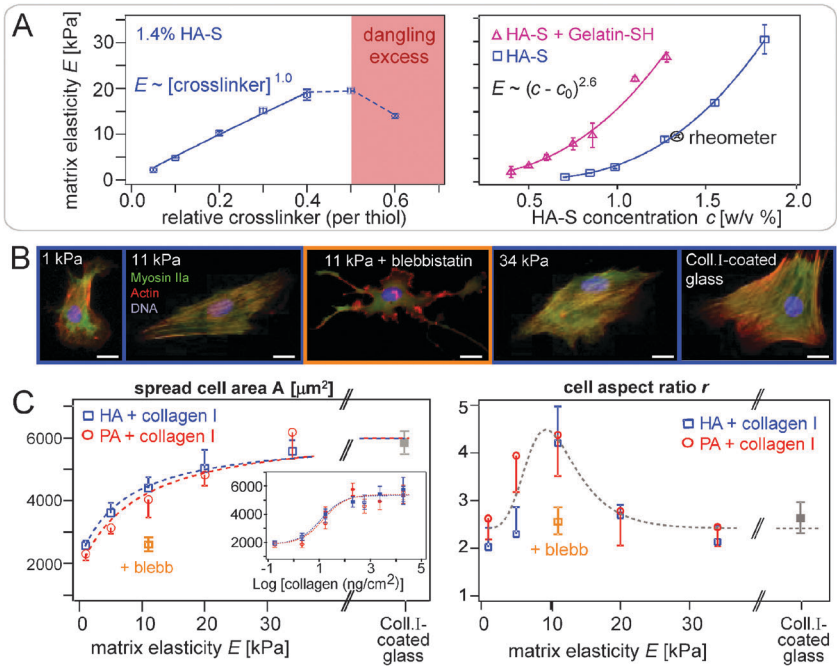

Fig. 2 The elasticity of HA and PA collagen-coated matrices both direct cell morphology in 2D (24 h), independent of material but dependent on myosin-II. (A) (Left) micro-elastic modulus E of HA gels measured by AFM (blue squares) scales linearly ($R^2 = 0.99$) with the amount of the cross-linker up to a critical cross-linker/thiol ratio of 0.5 beyond which the elasticity decreases due to dangling cross-linkers (shaded region). (Right) E of HA-S gels with a relative cross-linker ratio of 0.3 (blue squares) and HA-S + 1% gelatin-SH (purple triangles) both increase with HA-S concentration and are fitted by a scaling law (solid lines) with an exponent of 2.6 as expected for crosslinked polymer networks. The black circle with a cross depicts the shear modulus G' measured with a cone and plate rheometer that was converted to E assuming a Poisson's ratio of $\nu = 0.45$. (B) Fluorescence images of cells 24 h after plating on collagen-coated HA gels of different elasticity ($E = 1$, 11, and 34 kPa), collagen coated glass, and on a 11 kPa HA gel and treated with blebbistatin. Images represent average values of spread cell area A and cell aspect ratio r. (C) Matrix E dependent cell morphology of hMSCs. Plot of A on HA (blue squares) and PA (red circles) substrates of varying elasticity and glass (gray square) fitted per the text. Cells on 11 kPa HA gels treated with blebbistatin (orange square) exhibit a significantly smaller area. The inset shows that the spread cell area A increases with increasing surface concentration of collagen I fitted to binding isotherms with similar affinity constants. In the right plot, the cell aspect ratio r (major axis/minor axis of best-fit ellipse) shows a peak at 11 kPa for both hydrogel types and indicates more axisymmetric cell shapes on very soft and very rigid substrates as well as for blebbistatin treated cells on 11 kPa HA (orange square). Error bars are SEM.

MSC morphology is dictated by E beyond a ligand threshold

Plating hMSCs on the pure HA-S gels did not result in any significant adhesion or growth of healthy cells up to 48 hours, motivating the integration of gelatin noted above. Pure PA gels likewise do not permit cell adhesion, which again indicates that hMSCs are not able to secrete much matrix that adsorbs to and remodels either type of matrix. Collagen type I is the most abundant polymer in animals with adhesive motif(s) that are not completely clear; collagen I is frequently used to coat hydrogels for stable cell adhesion,[3,4,6] and its denatured derivative, gelatin, is also readily thiol-modified for incorporation into the HA gels here. The density of collagen not only determines the number of potential receptor ligands but can also influence the accessibility of HA. This is important because HA is known to interact with cell-surface receptors such as CD44 expressed on hMSCs; however, the HA-S here shows minimal binding to cells (Fig. S3, ESI‡). A systematic study of cell adhesion was therefore conducted while varying collagen concentration c on both PA and HA gels with a Young's modulus of $E = 11$ kPa (Fig. 2C, inset plot). With increasing collagen, the increase in the spread cell area A indicates increased binding with saturation at $A = A_0 + B = 5500 \pm 480$ μm^2, fitting a standard binding isotherm:

$$A = A_0 + Bc/[K + c]$$

Importantly, optimal curve fits for PA and HA substrates are nearly identical with affinity constants of $K_{HA} = 11 \pm 3$ ng cm^{-2} and $K_{PA} = 14 \pm 3$ ng cm^{-2}. For all subsequent experiments we used a collagen concentration well into the saturation regime, and we focused on steady state cell responses at 24 h as here unless indicated. Importantly, the results thus far suggest that the chemical nature of the underlying elastic scaffold (HA or PA) does not impact cell behavior.

To further elucidate potential differences between the HA gels and the more standard PA gel system, cells were plated on substrates of different elastic moduli E, fixed after 4 h or 24 h, and stained for actin, non-muscle myosin IIa (NMM IIa), and the nucleus. Fluorescence images of well-separated cells were used to determine the spread cell area A and the aspect ratio r (the ratio of major to minor axis of best-fit ellipse, also known as spindle factor). With matrix elasticity, A increases monotonically for both HA and PA as depicted in the left graph of Fig. 2C, with a maximum area A_{max} on collagen coated glass slips that can be considered infinitely rigid compared to the cell. Inhibition of nonmuscle myosin IIa (NMM IIa) with blebbistatin blocks the cell area and shape changes consistent with past studies over the entire physiological

range in E.[6] Indeed, if cell spreading is driven by the polymerization of actin and opposed by retrograde flow driven by myosin-based contraction that obeys the classic Hill equation (with highest velocity at lowest force), one can obtain a simple hyperbolic function for cell area A:

$$A = A_{max} - B/[k^m + E^m]$$

Characteristic constants that are obtained for both types of gel systems are very similar: $k_{HA} = 8.6 \pm 1$ kPa and $k_{PA} = 9.2 \pm 2$ kPa. The increase in cell area A agrees well with many studies,[2,3,6] and similar behavior on the two different systems shows that this response is indeed independent of matrix material.

The other morphological 'trait' analyzed is the aspect ratio r of the cell. While all cells start round (see below), they break this symmetry within hours for all E; but the right plot of Fig. 2C shows that r becomes maximal at $\sim$10 kPa. Again, the behavior on HA is analogous to PA substrates showing less elliptical cells on soft and rigid substrates and more elongated cells on matrices at an intermediate stiffness as reported in other recent studies.[6,31] Fitting r with a chemo-mechanical model that was developed originally for lineage induction (dashed grey line) yields a similar fit to that found previously with hMSCs.[6] Importantly, morphological changes of the type elaborated here proved to be a first, rapid step prior to subsequent lineage induction.

All of the morphological results above are indistinguishable with HA and PA gels coated with the same collagen I concentration. Keeping in mind that PA is completely synthetic and neutral whereas HA is nature-derived and polyanionic, cell responses are clearly to matrix mechanics.

pTyr signaling is maximal at intermediate E and targets myosin-II heavy chain

Prior to studying hMSCs in 3D culture with HA matrices, we sought insight into signaling pathways that might contribute to the nonmonotonic change in the cell shape with E (Fig. 2C). The seminal studies by Pelham and Wang[2] of matrix elasticity effects on cell lines (*versus* the primary cells here) had documented an overall lower amount of phosphotyrosine (pTyr) modified protein in cells on a soft matrix compared to a stiff matrix. Immunoblots here for pTyr in cells grown for 24 hours on matrices with E = 1, 11, and 34 kPa likewise reveal a tendency for less pTyr in cells on the softest matrix compared to the two stiffer matrices (Fig. 3A). However, there is also a statistically significant, $\sim$2-fold increase in pTyr in cells on a 11 kPa matrix (Fig. 3B) that is reminiscent of the $\sim$2-fold peak in aspect ratio r (Fig. 2C).

Among the bands in the pTyr immunoblot are high molecular weight bands that we thought might include an NMM IIa heavy chain, which has been reported to have at least one phospho-activated site in its motor domain and perhaps more in its tail that can impact filament assembly dynamics.[32] A direct study of NMM IIa included immunoprecipitation of either pTyr or NMM IIa and then probing for both pTyr and NMM IIa. The positive results here suggest that NMM IIa is indeed pTyr signal-activated more so on a 11 kPa matrix than on softer or rigid matrices.

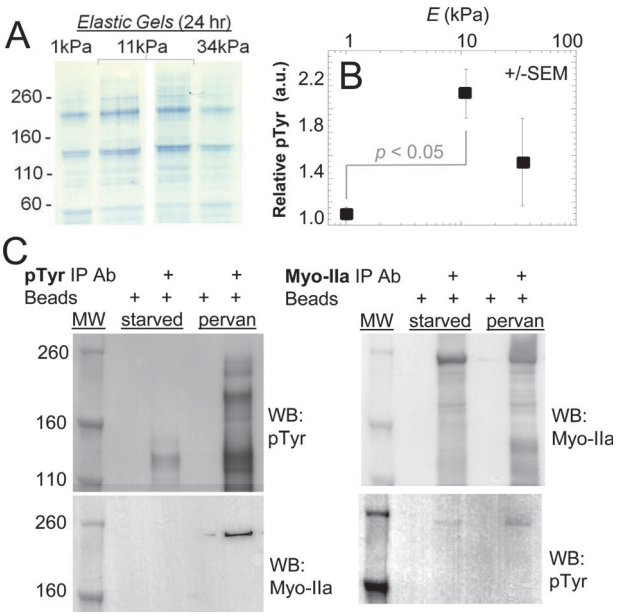

Fig. 3 pTyr signaling on elastic matrices is high on stiff matrices, especially a 11 kPa matrix, and includes nonmuscle myosin IIa among the targets. (A) Anti-pTyr immunoblot of hMSC lysates after 24 h cultures on various elastic PA substrates. (B) Relative amounts of pTyr based on densitometry of all bands above 100 kDa and relative to the same bands in the Coomassie stained gel ($n \geq 3$). (C) Immunoprecipitation (IP) and Western blotting (WB) for pTyr or NMM IIa, showing that the latter has pTyr. Since the band pattern appears similar for cells on all substrates (though not the band intensities), cells were grown on plastic to generate the large amounts of material needed for IP.

Conformal 3D environments with HA hydrogels

HA hydrogels can polymerize on or around living cells and thereby generate various 3D environments with well-controlled mechanical properties, but control over adhesion requires mixing the adhesive ligand into the hydrogel during gelation and covalently linking it to the HA. The thiol modified gelatin introduced above (Fig. 2A) is derived of course from heat-denatured, pyrolysed collagen that is very limited in fiber assembly capacity, and this is very different from the more common acid-derived collagen that can still assemble into collagen fibers under the correct conditions. The difference motivated a direct comparison, but first it had to be demonstrated that 2D substrates with increasing amounts of gelatin-SH show the expected sigmoidal increase in the spread cell area *versus* gelatin concentration (Fig. 4A). Working in the ligand saturation regime, cell morphology on 2D gels of HA that were either pre-mixed with gelatin-SH (HG) or else coated with collagen shows identical trends in the cell spread area and the aspect ratio (Fig. 4B). The results imply that collagen does not assemble into fibers, which is consistent with a lack of visible fibrils on the surface of a gel as imaged by AFM (Fig. 1B). Pre-exposure to serum does not affect these results (Fig. 4C). Given that cells do not spread on a low ligand matrix even in the presence of serum factors such as vitronectin, it is likely the integrated or attached ligand that controls cell adhesion and responses.

The use of HG gels on top of already spread cells establishes a conformal overlay as a 3D microenvironment for cells that

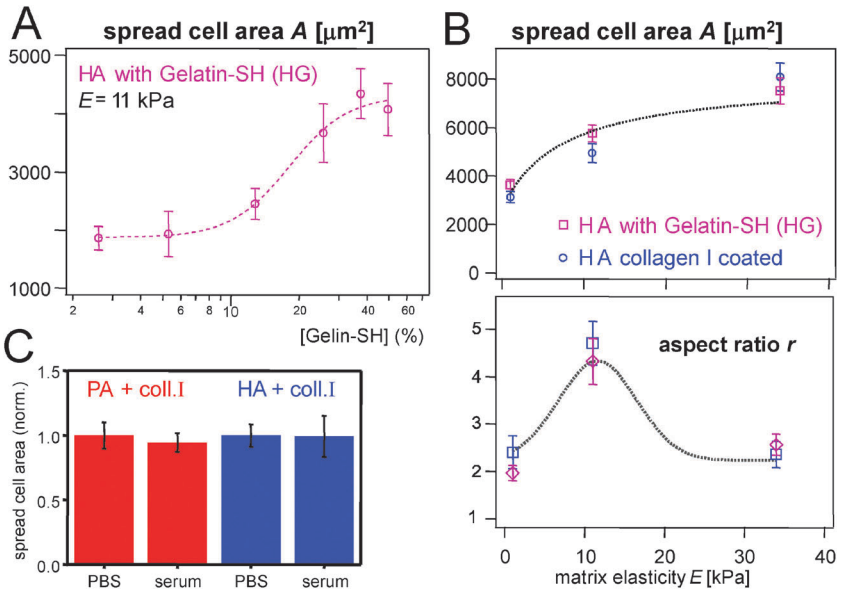

Fig. 4 Collagen I coatings and crosslink-integrated gelatin lead to similar cell behavior with no observable serum deposition effect. (A) Plot of spread cell area A at 24 h *versus* gelatin content [%] of a HA hydrogel. The binding isotherm is similar to that in the Fig. 2C inset. (B) A (top) and cell aspect ratio r (bottom) show similar behavior on collagen I coated HA-S and HA + Gelin-S hydrogels. (C) No significant difference in the spread cell area between HA gels (blue) and PA gels (red) pre-incubated for 24 h with serum compared to PBS controls used for normalization.

permit the study of cell morphology and cytoskeleton (Fig. 5A). The base hydrogel has elasticity E_{Lo} (1 or 11 kPa), and after time t (1 or 24 h) the second hydrogel of stiffness E_{Up} (1 or 11 kPa) is then carefully poured on top. Samples that were identically treated but not overlaid with a hydrogel were used as controls in analyses of cell area A and aspect ratio r. Cell spreading is essentially complete in 5–10 hours for soft or stiff matrices (Fig. 5B), but overlays perturb only the spreading on the stiff, 11 kPa matrix where the overlay leads to a significant reduction of the spread area. However, the cells round up asymmetrically upon overlay of the 11 kPa matrix: r increases significantly for both stiff and soft basal matrices (Fig. 5C). Furthermore, despite the non-equilibrium nature of such cell–matrix manipulations, no significant difference is seen with the two samples (1 kPa + 11 kPa) *versus* (11 kPa + 1 kPa). This indicates once again that the cell does not distinguish between upper and lower microenvironments and that the stiffer matrix dominates the cell response.

Overlaying a hydrogel at just 1 hour after plating was found to constrain the cell shape compared to cells in 2D (Fig. S4, ESI‡). Nonetheless, the kinetics of the major and the minor axes showed moderate increases that impacted spindle factor dynamics $r(t)$, which exhibited a time constant similar to the 2D control. In addition, to assess whether the increase in the spindle factor r was actively driven by actomyosin when the overlay was added at 24 hours, cells were treated with blebbistatin (an NMM II inhibitor) after the overlay, producing cells that lacked any organized actin stress fibers and that also had a smaller spindle factor which differed little from the 2D controls. Inhibition of myosin limits the contraction of the minor axis that is seen with untreated, sandwiched cells. The overlay also prevents the cell from randomly directed actin outgrowth that was seen for blebbistatin treated cells in 2D (Fig. 2B). The results all clearly indicate that cells use their actomyosin cytoskeleton to recognize matrix elasticity E in 3D.

Cytoskeletal order–disorder is dictated by E in 2D and 3D

The actomyosin network is physically linked through adhesions to the matrix and is a key player in mechano-response. Fluorescence images of immuno-stained NMM IIa were analyzed with a segmentation algorithm to calculate a nematic order parameter S that quantifies the relative alignment of stress fibers:[31] $S = 0$ is disordered or isotropic and $S = 1$ is completely aligned or ordered as a nematic. The disorder-to-order transition is nominally identified as $S = \frac{1}{2}$. Fig. 5D shows in the top row the orientation of actomyosin stress fibers of hMSCs cultured for 24 hours on 1, 11, and 34 kPa HA gels with different colors representing different directions. The order parameter S is low ($S = 0.2$–0.3) for both soft and rigid substrates in 2D cultures (Fig. 5D—i, plot), indicating an overall isotropic state for the cytoskeleton, but at intermediate matrix stiffness it reaches a maximum in the nematic regime ($S \approx 0.6$), indicating that the cytoskeleton is highly polarized and aligned. We recently developed a theoretical model[31] for cytoskeletal ordering in both 2D and 3D in which the cell is treated as an active elastic inclusion in a surrounding matrix and the actomyosin forces polarize in response to elastic stresses developed in the cell. In both $D = 2$ and 3, the response is the same generic form of a Lorentzian with matrix E scaled by cell elasticity (E_c):

$$S = a(E/E_c)/[(b(E - E_0)/E_c)^2 + 1]$$

The parameters a, b, E_0 are all functions of the aspect ratio r. They are also functions of cell polarizability (which can differ between cells), the Poisson ratio of the cell and matrix, and D of the system. The theory correctly predicts a non-monotonic dependence of S on E in 2D (Fig. 5D—(i), plot), and the following are the first studies of cells in 3D. For the same shape of cell (r), the theory shows that stress-fiber polarization in 2D

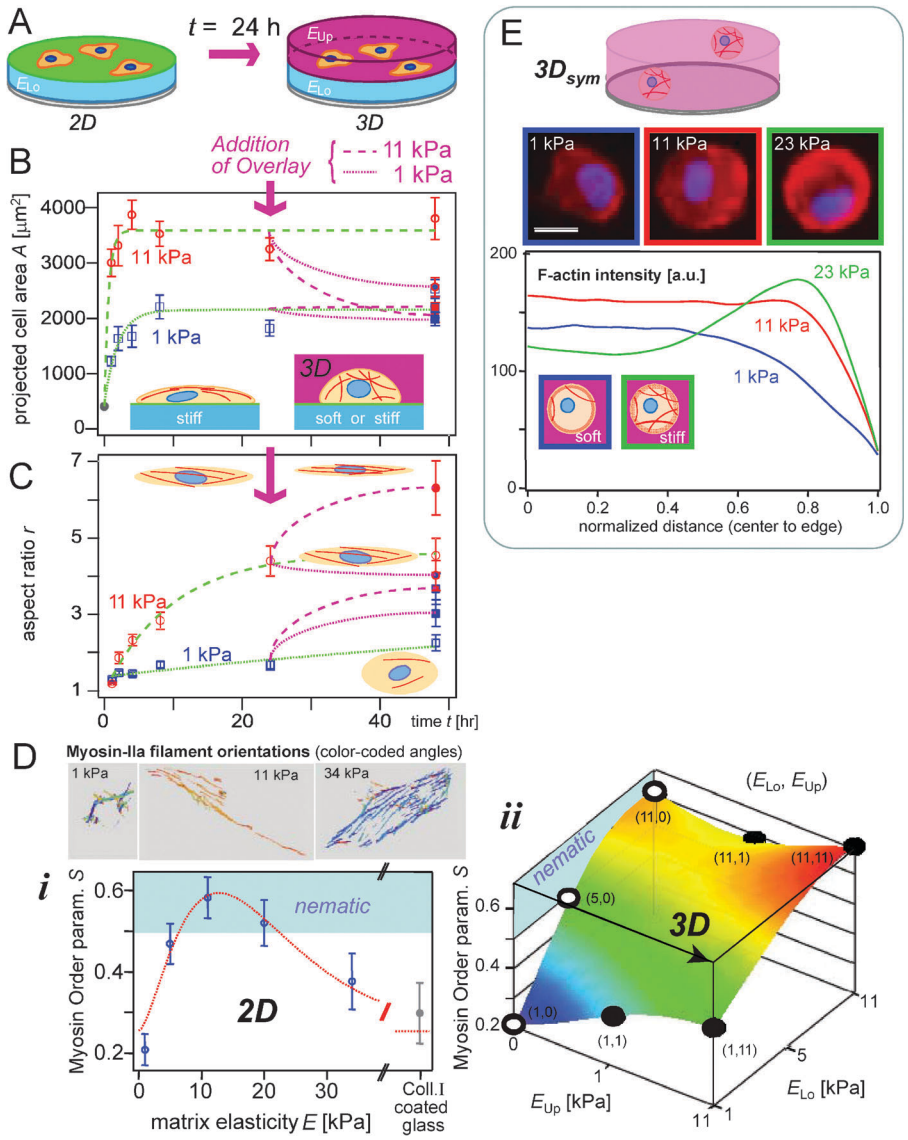

Fig. 5 In 3D, stiffness and asymmetry of matrices direct cell shape and cytoskeletal organization. (A) Sketch of the sandwich overlay procedure. Cells were plated on a collagen I coated base hydrogel of elasticity E_{Lo} and after time $t = 24$ h a second hydrogel of stiffness E_{Up} was polymerized on top to create a fully conformal 3D overlay. (B) The graph shows the kinetics of the spread cell area A for two different elasticities of the lower matrix (longer dashed green line 11 kPa, shorter dashed green line 1 kPa). On 2D substrates the spreading process is nearly complete after 4 h. Overlay (purple arrow) of different upper gels (purple dashed lines) onto the 11 kPa substrates leads to major decreases in the cell area. In contrast, overlays on 1 kPa substrates have a minimal impact on A. (C) The cell aspect ratio r of the same cells as in (B) increases with either overlay for 1 kPa substrates. However, r increases only with a 11 kPa overlay when cells are on a 11 kPa substrate, with the sketched shape indicating a narrowing of the cell. (D) Top row shows the orientation of stress fibers in cells on 1, 11, and 34 kPa HA gels as determined by a segmentation algorithm with different colors representing different directions; the order parameter was calculated using the 2D projection of myosin-IIa fibers on the substrate.[31] (i) Plot of the myosin-IIa order parameter S *versus* matrix E shows a maximum near 11 kPa. (ii) Surface plot of S for the different sandwich configurations as well as 2D (where $E_{Up} = 0$ kPa). Differences due to substrate elasticity with added overlay (E_{Lo}, E_{Up}) are significant in the case of (1, 1) with $p < 0.05$. Mirror symmetric conditions (1, 11) and (11, 1) are not significantly different. (E) Encapsulated hMSCs in 3D HA hydrogels with fluorescence images (red—actin, blue—nucleus). The plot shows the radial intensity distribution of actin indicating an increasing actin concentration at the cell cortex with increasing stiffness (mean profiles shown for $n \geq 5$ cells with SEM $\leq 10\%$ of mean signal; differences between 1 kPa and 23 kPa are significant at every data point).

is larger by a factor of ~ 2 compared with 3D where the surrounding matrix suppresses the anisotropy of the elastic stress in the cell. However, in the present case the overlay drives a morphology change that increases r, and our previous calculations show that with matrix $E > 1$ kPa, S is more than doubled (see Fig. 4a in ref. 31), which should more than offset the tendency of the 3D matrix to suppress the cytoskeletal order.

For cells in our overlay cultures, the higher dimensional matrix indeed promotes cell elongation and cytoskeletal order (Fig. 5D—(ii), plot). Adding a 1 kPa overlay to the 1 kPa base gel significantly ($p < 0.05$) increases the cytoskeletal order from $S \approx 0.2$ (2D) to $S \approx 0.35$ (3D), although the cytoskeleton remains well below the nematic order. While adding the same 1 kPa overlay to a 11 kPa gel has no significant effect on S,

adding a 11 kPa overlay to a soft base matrix of 1 kPa increases the order dramatically even more ($p < 0.01$), driving the isotropic cytoskeleton very close to the nematic regime with $S \approx 0.45$. Adding the same overlay 11 kPa to a 11 kPa base gel increases the cytoskeletal order slightly to $S \approx 0.7$, consistent with enhancement of the order by a more spindle-like shape with higher r.[31] Importantly, the two mirror symmetric samples (1, 11 kPa) and (11, 1 kPa) are not significantly different ($p > 0.05$) indicating that the cell does not distinguish between basal and apical matrices, despite the major differences in the overlay process.

Lastly, cells were encapsulated in homogeneous 3D HG gels in a single step ($3D_{sym}$; Fig. 5E, sketch). In both HG and HA gels, a metabolism assay (WST-1, Roche Applied Science) showed that cells are viable and can proliferate. Long term experiments showed viability of such encapsulated cells for about a month, and when the matrix was degraded overnight with hyaluronidase the released cells started to spread normally on glass. After just 24 h, cells in $3D_{sym}$ show little dependence of the projected cell area on gels of different elasticity E, which is fully consistent with the 3D overlay results (Fig. 2B) and distinct of course from 2D where cell areas differ greatly (Fig. 2C, 4B, and 5B). However, this type of polymerization tends to cage and confine the cells, thus giving $r \approx 1$. Nonetheless, F-actin seems to increase in amount with increasing E, consistent with our model,[31,33] and it also shifts to the cortex with increasing E (Fig. 5E, plot). This cytoskeletal result is the spherically-symmetric limit to the matrix elasticity-driven increases in the contractile stress fiber order shown above in cells with much higher r in 3D overlays (Fig. 5C and D).

Conclusions

Fine tuning of both the matrix elasticity and ligand density of thiol-modified HA allows one to cover a broad range of physiologically relevant stiffness. With such control, stem cell morphologies are indistinguishable on PA and HA matrices, which underscores many past conclusions that the mechano-sensitivity of cells to matrix elasticity is a general biophysical response independent of matrix material. The thiol functionalities also allow for coupling of a variety of molecules to the matrix as demonstrated here with thiol-modified gelatin as well as the maleimide dye for imaging an overlay (Fig. 1D).

Cell morphology and cytoskeletal order in 3D (Fig. 4 and 5) demonstrate that elasticity E dictates cell state with nonmonotonic mechanics and with a likely basis in E-dependent activation of nonmuscle myosin (Fig. 3). When cells are conformally overlaid at a very early time point or simply embedded (as many groups do) the polymer chains constrain the cell shape (to $r \approx 1$) and prevent the usual symmetry breaking since the cell cannot remodel such hydrogels on short timescales (of days). A cortical cytoskeleton develops nonetheless in response to stiffer matrices, but it does not polarize, consistent with theory.[31] Fibrillar 3D systems add complexity to understanding such processes but they are porous and hydrophilic like physiological matrices. In comparison, PDMS microwells of 20 kPa that impose $r \approx 1$ suppress stress fiber assembly[15] as expected from theory[31] and motivate further study of such hydrophobic materials in quasi-3D geometries, perhaps with microwells where $r \gg 1$. Given the importance of rapid, cytoskeleton-driven morphology changes in processes such as lineage induction,[6] the physical properties of cellular micro-environments in 2D and 3D seem essential to control and understand.

Materials and methods

Hyaluronic acid hydrogel preparation

Hyaluronic acid (HA, M_w = 413 kDa) obtained from Lifecore Biomedical (Chaska, MN) was functionalized with thiol groups by adapting the protocol reported by the group of Prestwich.[23] In brief, 3-(2-pyridyldithio)propionyl hydrazide (PDPH) (Pierce) was coupled to the carboxyl group of HA using carbodiimide chemistry. Using PDPH, a monofunctional reagent, instead of the homo-bifunctional dithiobis(propanoic dihydrazide) (DTP) avoids cross-linking of HA during the reaction that could lead to inhomogeneous modification favoring proximal intra-molecular crosslinks. Then the disulfide bonds of PDPH were reduced using dithiothreitol (DTT) with subsequent dialysis (cut-off M_w = 10 kDa) to purify the thiolated HA (HA-S) followed by lyophilization. The degree of substitution of HA-S was determined by ^{1}H NMR in D_2O using a 360 MHz instrument (BZH 360/52, Spectrospin and Oxford instruments). For the 3D hydrogels Gelin-S (thiol-modified gelatin) was used, a kind gift from Glycosan (Salt Lake City, UT) and recombinant gelatin (100 kDa, full length) was modified in a similar manner as HA.

Hydrogels were prepared on cover slips (25 mm diam., Fisher Scientific) as a solid support to facilitate culture, imaging, and elasticity measurements. Polyacrylamide (PA) hydrogels were prepared as control samples and both gel systems were coated with collagen I (BD Biosciences) using the heterobifunctional crosslinker Sulfo-SANPAH (Pierce) as described elsewhere.[2,6,19] Collagen I surface density was determined per ref. 3.

Hydrogel sandwich preparation

The whole procedure is performed in a biosafety cabinet to maintain sterility. All equipment used was either sterile or sterilized by UV treatment for one hour. Cells were cultured for a given time on 2D substrates, rinsed with PBS and bulk liquid removed. 35 μl of the hydrogel mixture was added immediately and the sample was covered with a hydrophobic chlorosilanized glass slip to create a homogenous overlay gel. After one hour the top cover slip was carefully removed and the sandwich rinsed with PBS to remove any unbound residue. Subsequently, the gels were incubated for two hours at 37 °C/5.0% CO_2 in media supplemented with 2% cysteine (w/v) to cap any remaining free thiols. Finally, the hydrogel was washed with media and maintained under the usual cell culture conditions.

To fluorescently label the sandwich overlay, it was rinsed following gelation and then incubated while gently rocking for 2.5 min with 2 ml of a 0.4 μg ml^{-1} solution of Alexa-647 maleimide (Invitrogen) in PBS while gently rocking for 2.5 min, followed by twice rinsing the gels with PBS.

Measuring Young's elastic modulus E

Elasticity measurements on the hydrogels were performed with MFP-1D and MFP-3D AFMs (Asylum Research, Santa Barbara, CA). Force-indentation curves were recorded using cantilevers with a pyramidal tip and a nominal spring constant

$k = 0.06$ N m^{-1} (DNP, Veeco, Santa Barbara, CA), which was calibrated by the thermal tune method.[34] The Young's modulus E was calculated using a Hertz type model assuming a Poisson ratio of $\nu = 0.45$[12,28] and a pyramidal indenter:

$$E = \pi(1 - \nu^2)\, F/[\delta^2(2 \tan \alpha)]$$

Measurements were also done using cantilevers with a sphere attached on the tip (borosilicate spheres; Novascan) of radius $R = 2.5$ μm, which led to similar values for E using:

$$E = 3(1 - \nu^2)F/[4\delta^{3/2}R^{1/2}]$$

Bulk measurements were performed with an RFS II cone (1°, 25 mm diameter) and a plate rheometer (TA Instruments, New Castle, DE). Shear modulus G' proved independent of applied strain up to 25% in accordance with Ghosh *et al.*[20] In addition, the measured viscous contribution proves very small with $G'' \approx G'/11$ for the 11 kPa HA gel. For a PA gel of similar elasticity, $G'' \approx G'/20$, indicating that both gel types are predominantly elastic. Cell responses to viscosity are likely to be better studied with far more viscous matrices. For conversion of G' to E a Poisson's ratio of $\nu = 0.45$ was assumed in:

$$E = 2G'(1 + \nu).$$

Because this last equation depends linearly on ν whereas the equations used in AFM depend quadratically on ν, there is a finite range of ν that gives results for E within about 10% by both rheometry and AFM. A value of $\nu = 0.45$ is in the middle of that range (0.4–0.5). This result is also consistent with the strong tendency of these hydrogels to retain water, which is incompressible. Based on three means of measuring E, its accuracy is also $\leq 10\%$.

Acknowledgements

The authors thank NIH (P01DK032094, R01HL062352) and NSF (NSEC, MRSEC) for support, the three reviewers and Dr Mina Bissell for comments, Dr A. Scott and Dr G. Prestwich for discussions, and Glycosan for Gelin-S and Glycosil. F. R. is grateful for financial support through a Feodor Lynen fellowship from the Alexander von Humboldt foundation and thanks N. Cohen for experimental assistance and A. Rehfeldt for illustrations as well as Dr D. A. Christian for help with confocal microscopy and Dr K. Rajagopal for NMR measurements. A. Z. thanks the Israel Science Foundation for their support.

Notes and references

1 D. E. Discher, P. Janmey and Y. L. Wang, *Science*, 2005, **310**, 1139–1143.
2 R. J. Pelham and Y. L. Wang, *Proc. Natl. Acad. Sci. U. S. A.*, 1997, **94**, 13661–13665.
3 A. Engler, L. Bacakova, C. Newman, A. Hategan, M. Griffin and D. Discher, *Biophys. J.*, 2004, **86**, 617–628.
4 A. Kostic, J. Sap and M. P. Sheltz, *J. Cell Sci.*, 2007, **120**, 3895–3904.
5 C. M. Lo, H. B. Wang, M. Dembo and Y. L. Wang, *Biophys. J.*, 2000, **79**, 144–152.
6 A. J. Engler, S. Sen, H. L. Sweeney and D. E. Discher, *Cell*, 2006, **126**, 677–689.
7 F. Rehfeldt, A. J. Engler and D. E. Discher, in *V: Nanomedicine*, ed. V. Vogel, Wiley VCH, 2009.
8 M. J. Paszek, N. Zahir, K. R. Johnson, J. N. Lakins, G. I. Rozenberg, A. Gefen, C. A. Reinhart-King, S. S. Margulies, M. Dembo, D. Boettiger, D. A. Hammer and V. M. Weaver, *Cancer Cell*, 2005, **8**, 241–254.
9 J. M. Goffin, P. Pittet, G. Csucs, J. W. Lussi, J. J. Meister and B. Hinz, *J. Cell Biol.*, 2006, **172**, 259–268.
10 J. W. Shin, J. Swift, K. R. Spinler and D. E. Discher, *Proc. Natl. Acad. Sci. U. S. A.*, 2011, **108**, 11458–11463.
11 P. M. Gilbert, K. Havenstrite, K. E. Magnusson, A. Sacco, N. A. Leonardi, P. Kraft, N. K. Nguyen, S. Thrun, M. P. Lutolf and H. M. Blau, *Science*, 2010, **329**, 1078–1081.
12 F. Rehfeldt, A. J. Engler, A. Eckhardt, F. Ahmed and D. E. Discher, *Adv. Drug Delivery Rev.*, 2007, **59**, 1329–1339.
13 A. I. Caplan and D. Correa, *Cell Stem Cell*, 2011, **9**, 11–15.
14 R. Merkel, N. Kirchgebner, C. M. Cesa and B. Hoffmann, *Biophys. J.*, 2007, **93**, 3314–3323.
15 M. Ochsner, M. Textor, V. Vogel and M. L. Smith, *PLoS One*, 2010, **5**, e9445.
16 F. Grinnell, *Trends Cell Biol.*, 2003, **13**, 264–269.
17 H. K. Kleinman and G. R. Martin, *Semin. Cancer Biol.*, 2005, **15**, 378–386.
18 S. Kuang, M. A. Gillespie and M. A. Rudnicki, *Cell Stem Cell*, 2008, **2**, 22–31.
19 A. J. Engler, F. Rehfeldt, S. Sen, D. E. Discher, in *Methods in Cell Biology*, ed. Y. L. Wang and D. E. Discher, Academic Press, 2007, pp. 521–545.
20 K. Ghosh, X. Z. Shu, R. Mou, J. Lombardi, G. D. Prestwich, M. H. Rafailovich and R. A. F. Clark, *Biomacromolecules*, 2005, **6**, 2857–2865.
21 J. A. Burdick, C. Chung, X. Q. Jia, M. A. Randolph and R. Langer, *Biomacromolecules*, 2005, **6**, 386–391.
22 B. Ananthanarayanan, Y. Kim and S. Kumar, *Biomaterials*, 2011, **32**, 7913–7923.
23 X. Z. Shu, Y. C. Liu, Y. Luo, M. C. Roberts and G. D. Prestwich, *Biomacromolecules*, 2002, **3**, 1304–1311.
24 S. S. Cai, Y. C. Liu, X. Z. Shu and G. D. Prestwich, *Biomaterials*, 2005, **26**, 6054–6067.
25 Y. C. Liu, X. Z. Shu and G. D. Prestwich, *Biomaterials*, 2005, **26**, 4737–4746.
26 X. Z. Shu, Y. C. Liu, F. S. Palumbo, Y. Lu and G. D. Prestwich, *Biomaterials*, 2004, **25**, 1339–1348.
27 A. J. Engler, L. Richert, J. Y. Wong, C. Picart and D. E. Discher, *Surf. Sci.*, 2004, **570**, 142–154.
28 J. Domke and M. Radmacher, *Langmuir*, 1998, **14**, 3320–3325.
29 P. J. Flory, *Principles of Polymer Chemistry*, Cornell University Press, Ithaca, 1953.
30 C. Storm, J. J. Pastore, F. C. MacKintosh, T. C. Lubensky and P. A. Janmey, *Nature*, 2005, **435**, 191–194.
31 A. Zemel, F. Rehfeldt, A. E. X. Brown, D. E. Discher and S. A. Safran, *Nat. Phys.*, 2010, **6**, 468–473.
32 R. K. Tsai and D. E. Discher, *J. Cell Biol.*, 2008, **180**, 989–1003.
33 A. Zemel, F. Rehfeldt, A. E. X. Brown, D. E. Discher and S. A. Safran, *J. Phys.: Condens. Matter*, 2010, **22**, 194110.
34 J. L. Hutter and J. Bechhoefer, *Rev. Sci. Instrum.*, 1993, **64**, 1868–1873.

